Image-Based Non-rigid Body Mechanical Property Recovery
Dissertation Proposal

Shan Yang

University of North Carolina at Chapel Hill
November 21, 2016

1 Introduction

Non-rigid bodies are widely used in computer graphics, medical robotics, design and manufacturing, virtual surgery for soft robot planning, procedural rehearsal and training, virtual try-on etc. Identification of mechanical properties, such as tissue elasticity parameters, is critical to enable medical robots to safely operate within highly unstructured, deformable human bodies and to compute desired, accurate force feedback for individualized haptic display characterized by patient-specific parameters. Studies have shown that the tissue stiffness described by the tissue properties may indicate abnormal pathological process. *Ex-vivo*, measurement-based methods, such as [1,12] using magnetic resonance imaging (MRI) and/or ultrasound, were proposed for study of prostate cancer tissue. However, previous works in material property reconstruction often have limitations with respect to their genericity, applicability, efficiency and accuracy [35]. Also, in virtual realty applications such as virtual try-on system for clothing, it is important to recreate the material properties of the garment; accurate recreation of the fabric not only gives a better visual simulacrum of the cloth, but also affects how the garment feels and fits on the body.

The goal of this work is a coupled physically-based simulation optimization method to recover soft body mechanical properties from images or videos.

2 Thesis Statement

Material properties of the non-rigid objects presented in images or videos can be estimated using a simulation optimization coupled or a machine learning based method.

3 Expected Contributions

In defense of this thesis statement, I intend to offer following contributions:

- **Image-based multi-region mechanical property recovery:** A method to recover material properties of multiple regions of a deformable body.
- **Video-based dynamic non-rigid body mechanical property recover:** A method to recover the material properties of the soft body given a video which records the motion of it.

- **Mechanical property recovery for cancer stage correlation study:** Study the correlation between the recovered mechanical property of the human organ and its cancer stage/score.
- **Video-based garment mechanical property recovery:** A method to recover the material property of a garment based on the video which records the motion of it.

4 Related Prior Work

Physically-based deformable body simulation has been extensively studied in computer graphics for decades [16,18,28,39]. Here we briefly discuss prior work on the estimation of material parameters. Parameter estimation has received increasing attention in computer graphics for its uses in rendering, modeling, and simulating different materials. Pai *et al*. integrated a force measurement device with a trinocular stereo system to model the material properties of deformable objects by estimating the linear relationship between displacements and tractions using a least-squares formulation [20]. Other methods have combined a force sensor with a trinocular stereo vision system to measure the forces applied and the displacements of the vertices on the deformable surface; these measurements are then used to determine the nonlinear heterogeneous material properties [5]. Syllebranque *et al*. [27] used a force-capture device to measure boundary forces and estimate the mechanical properties of deformable solids. By using video-based metrics to optimize for Poisson's ratio and for the errors in computed boundary forces, their method optimized the value of Young's modulus.

Other mechanical property recovery methods have focused on physically-based simulation of cloth, especially on determining the cloth model's stiffness and damping coefficients. [4] estimated cloth simulation parameters by comparing video of real fabric patches with simulated images; they used the orientation of each edge pixel to compute the error metric, and used the continuous simulated annealing method [21] to minimize estimation error. Becker and Teschner presented a novel framework based on quadratic programming to determine linear elastic parameters; they also assessed the effects of noisy measurements [3]. Most recently, improved data-driven methods have been proposed to estimate cloth parameters [31,14,15], which can photorealistically recreate the look of real fabric.

Estimation of material parameters for human tissues is also well-studied in medical image analysis, where it is used in screening and detecting tumors, as cancerous tissues tend to be stiffer than healthy tissues. A non-invasive method, 2D elastography (also known as elasticity reconstruction), can acquire 'strain images' or 'elasticity images' of soft tissues [26]. Elastography is usually done by estimating the optimal deformation field that relates two ultrasound images, one taken at the rest state and the other taken when a known force is applied to the skin [19,22]. Alternatively, the displacement field can be found with a modified MRI machine that is in tune with a mechanical vibration of tissues [17,9]. Assuming that the physical model is linear, once the deformation field and external forces are known, the material properties can be computed by simply solving a least-squares problem [38] or by performing an iterative optimization to minimize the error in the deformation field [11,2,25]. Although these iterative methods are slower than directly solving the inverse problem, iterative methods are suitable for any

physical model, since they do not require linearity of the underlying tissue model. [32] present an alternative 2D elastography for extracting tissue parameters. 3D elastography usually requires force measurements, but it is not always possible to obtain these measurements for deeply-seated organs, such as the prostate.

5 Achievements

I proposed an iterative simulation-optimization-identification framework consists of two alternating phases: the forward simulation to estimate the tissue deformation and inverse process that refines the tissue elasticity parameters to minimize the error in a given objective function. The input to our framework are two sets of 3D images. After iterations of the forward and inverse processes, we obtain the best set of elasticity parameters. Below we provide a brief overview of the key steps in this framework.

I applied this iterative simulation-optimization approach to the mechanical properties of human organs. And I did a mechanical property and cancer stage/score correlation study. The study shows that the recovered mechanical property can be used for cancer stage/score prediction. Further I proposed simulation-graphical model coupled framework to recover material parameters of a dynamic soft body.

In the following sections, I will illustrate the iterative simulation-optimization-identification framework, cancer correlation study and simulation-graphical model coupled framework.

5.1 Forward Simulation: Soft Body Modeling

In our system, we apply Finite Element Method (FEM) and adopt Mooney Rivlin material for bio-tissue modeling [6]. After discretization using FEM, we arrive at a linear system,

$$\mathbf{K}\mathbf{u} = \mathbf{f} \tag{1}$$

with $\mathbf{K}$ as the stiffness matrix, $\mathbf{u}$ as the displacement field and $\mathbf{f}$ as the external forces. The stiffness matrix $\mathbf{K}$ is not always symmetric possitive definite due to complicated boundary condition. The boundary condition we applied is the traction forces (shown in Fig. 7(a) of the supplementary document) computed based on the displacement of the surrounding tissue (overlapping surfaces shown in Fig. 7(b) of the supplementary document). We choose to use the Generalized Minimal Residual (GMRES) [24] solver to solve the linear system instead of the Generalized Conjugate Gradient (GCG) [13], as GMRES can better cope with non-symmetric, positive-definite linear system.

The computation of the siffness matrix $\mathbf{K}$ in Eqn. 1 depends on the energy function $\boldsymbol{\Psi}$ of the Mooney Rivlin material model [23,29].

$$\boldsymbol{\Psi} = \frac{1}{2}\mu_1((\mathbf{I}_1^2 - \mathbf{I}_2)/\mathbf{I}_3^{\frac{2}{3}} - 6) + \mu_2(\mathbf{I}_1/\mathbf{I}_3^{\frac{1}{3}} - 3) + v_1(\mathbf{I}_3^{\frac{1}{2}} - 1)^2, \tag{2}$$

where μ_1, μ_2 and v_1 are the material parameters. In this paper, we recover parameters μ_1 and μ_2. Since prostate soft tissue (without tumors) tend to be homogenous, we use the average $\bar{\mu}$ of μ_1 and μ_2 as our recovered elasticity parameter. v_1 is linearly related to the bulk modulus. The larger the bulk modulus, the more incompressible the object.

Relative Elasticity Value: In addition, we divide the recovered absolute elasticity parameter $\bar{\mu}$ by the that of the surrounding tissue to compute the relative elasticity parameter $\hat{\mu}$. This individualized relativity value helps to remove the variation in mechanical properties of tissues between patients, normalizing the per-patient fluctuation in absolute elasticity values due to varying degrees of hydration and other temporary factors. We refer readers to our supplementary document for details regarding non-linear material models.

5.2 Inverse Process: Optimization for Parameter Identification

To estimate the patient-specific relative elasticity, our framework minimizes the error due to approximated parameters in an objective function. Our objective function as defined in Eqn. 3 consists of the two components. The first part is the difference between the two surfaces – one reconstructed from the reference (initial) set of images, deformed using FEM simulation with the estimated parameters toward the target surface, and one target surface reconstructed from the second set of images. This difference is measured by the Hausdorff distance [7]. In addition we add a Tikhonov regularization [8,10] term, which improves the conditioning of a possibly ill-posed problem.

With regularization, our objective function is given as:

$$\boldsymbol{\mu} = \underset{\boldsymbol{\mu}}{\operatorname{argmin}} \sum \|\mathbf{d}(\mathbf{S}_l, \mathbf{S}_t)\|^2 + \lambda \boldsymbol{\Gamma} \mathbf{S}_l, \tag{3}$$

with $\mathbf{d}(\mathbf{S}_l, \mathbf{S}_t)$ as the distance between deformed surface and the reference surface, λ as the regularization weight, and $\boldsymbol{\Gamma}$ as the second-order differentiatial operator.

The second-order differential operator $\boldsymbol{\Gamma}$ on a continuous surface (2-manifolds) $\mathbf{S}$ is the curvatures of a point on the surface. The curvature is defined through the tangent plane passing that point. We denote the normal vector of the tangent plane as $\mathbf{n}$ and the unit direction in the tangent plane as $\mathbf{e}_\theta$. The curvature related to the unit direction $\mathbf{e}_\theta$ is $\kappa(\theta)$. The mean curvature κ_{mean} for a continuous surface is defined as the average curvature of all the directions, $\kappa_{mean} = \frac{1}{2\pi} \int_0^{2\pi} \kappa(\theta) \mathrm{d}\theta$. In our implementation, we use triangle mesh to approximate a continuous surface. We use the 1-ring neighbor as the region for computing the mean curvature normal on our discrete surface $\mathbf{S}_l$. We treat each triangle of the mesh as a local surface with two conformal space parameters u and v. With these two parameters u and v the second-order differential operator $\boldsymbol{\Gamma}$ on vertex $\mathbf{x}$ is, $\Delta_{u,v}\mathbf{x} = \mathbf{x}_{uu} + \mathbf{x}_{vv}$.

5.3 Recovered Mechanical Property for Cancer Stage/Score Correlation Study

Preprocessing and Patient Dataset Given the CT images (shown in Fig. 1a) of the patient, the prostate, bladder and rectum are first segmented in the images. Then the 3D surfaces (shown in Fig. 1b) of these organs are reconstructed using VTK and these surfaces would be the input to our elasticity parameter reconstruction algorithm. Our patient dataset contains 113 (29 as the reference and 84 as target) sets of CT images from 29 patients, each patient having 2 to 15 sets of CT images. Every patient in the dataset has prostate cancer with cancer T-stage ranging from T1 to T3, Gleason score ranging from 6 to 10, and age from 50 to 85. Gleanson scores are usually used to assess the aggressiveness of the cancer.

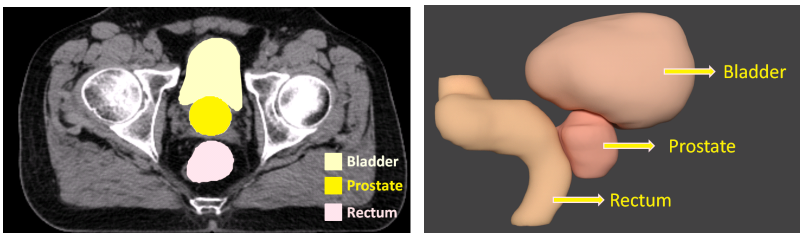

(a) (b)

Fig. 1. Real Patient CT Image and Reconstructed Organ Surfaces. (a) shows one slice of the parient CT images with the bladder, prostate and rectum segmented. (b) shows the reconstructed organ surfaces.

Cancer Grading/Staging Classification based on Prostate Elasticity Parameters We further study the feasibility of using recovered elasticity parameters as a cancer prognostic indicator using our classifier based on relative tissue elasticity values and ages. Two classification methods, ordinal logistic regression and multinomial logistic regression, were tested in our study. We test each method with two sets of features. The first set of features contains only the relative tissue elasticity values $\hat{\mu}$. The resultant feature vector is one dimension. The second set of features contains both the relative tissue elasticity values and the age. The feature vector for this set of features is two dimensional. Our cancer staging has $C = 3$ classes, T1, T2 and T3. And the cancer grading has $G = 5$ classes, from 6 to 10. In our patient dataset, each patient has at least 2 sets of CT images. The elasticity parameter reconstruction algorithm needs 2 sets of CT images as input. We fix one set of CT images as the initial (reference) image and use the other M number of images $\mathcal{T}, where|\mathcal{T}| = M$ as the target (deformed) images. By registering the initial image to the target images, we obtain one elasticity parameter $\hat{\mu}_i, i = 1 \dots M$ for each image in $\mathcal{T}$. We perform both per-patient and per-image cross validation.

Per-Image Cross Validation: We treat all the target images ($N = 84$) of all the patients as data points of equal importance. The elasticity feature for each target image is the recovered elasticity parameter $\hat{\mu}$. In this experiment, we train our classifier using the elasticity feature of the 83 images then cross validate with the one left out. Then, we add the patient's age as another feature to the classifier and perform the validation. The results for cancer staging (T-Stage) classification are shown in Fig. 2a and that for cancer grading (Gleason score) classification are shown in Fig. 2b. The error metric is measured as the absolute difference between the classified cancer T-Stage and the actual cancer T-Stage. Zero error-distance means our classifier accurately classifies the cancer T-Stage.

The multinomial method outperforms the ordinal method for both cancer staging (T-Stage) and cancer aggression (Gleason score) classification. The main reason that we are observing this is due to the optimization weights or the unknown regression coefficients $\boldsymbol{\beta}$ (refer to supplementary document for the definition) dimension of the multinomial and ordinal logistic regression method. The dimension of the unknown regression coefficients of the multinomial logistic regression for cancer staging classification (with elasticity parameter and age as features) is 6 while that of ordinal logistic

regression is 4. With the 'age' feature, we obtain up to $\mathbf{91}\%$ accuracy for perdicting cancer T-Stage using multinomial logistic regression method and $\mathbf{89}\%$ using ordinal logistic regression method. For Gleason score classification we achieve up to $\mathbf{88}\%$ accuracy using multinomial logistic regression method and $\mathbf{81}\%$ using ordinal logistic regression method.

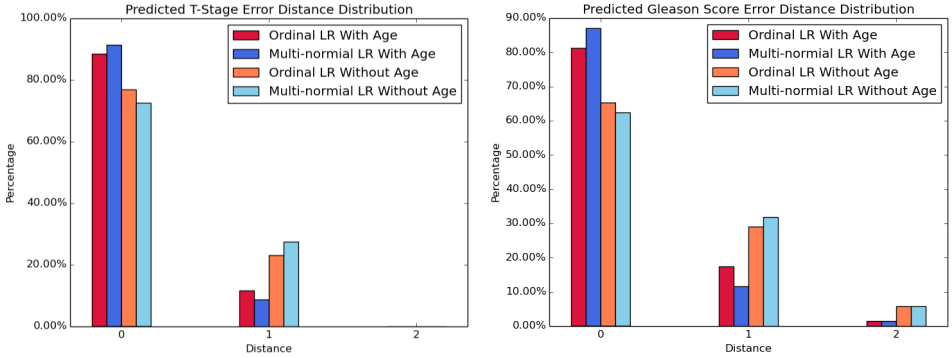

(a) (b)

Fig. 2. Error Distribution of Cancer Grading/Staging Classification for Per-Image Study. (a) shows error distribution of our cancer staging classification using the recovered prostate elasticity parameter and the patient's age. For our patient dataset, the multinomial classifier (shown in royal blue and sky blue) outperforms the ordinal classifier (shown in crimson and coral). We achieve up to $\mathbf{91}\%$ accuracy using multinomial logistic regression and $\mathbf{89}\%$ using ordinal logistic regression for classifying cancer T-Stage based on recovered elasticity parameter and age. (b) shows the correlation between the recovered relative elasticity parameter and the Gleason score with/without the patient's age. We achieve up to $\mathbf{88}\%$ accuracy using multinomial logistic regression and $\mathbf{81}\%$ using ordinal logistic regression for classifying Gleason score based on recovered elasticity parameter and age.

Per-Patient Cross Validation: For patients with more than 2 sets of images, we apply Gaussian sampling to $\hat{\mu}_i, i = 1 \ldots M$ to compute the sampled elasticity parameter as the elasticity feature of the patient. We first train our classifier using the elasticity feature of the 28 patients then test the trained classifier on the remaining one patient not in the training set. We repeat this process for each of the 29 patients. Then we include the patient age as another feature in the classifier. The error distribution for cancer staging (T-Stage) classification results are shown in Fig. 3a and the error distribution of cancer grading (Gleason score) classification are shown in Fig. 3b. We observe that the multinomial method in general outperforms the ordinal method. More interestingly, the age feature helps to increase the classification accuracy by 2% for staging classification and 7% for Gleason scoring classification). With the age feature, our multinomial classifier achieves up to $\mathbf{84}\%$ accuracy for classifying cancer T-Stage and up to $\mathbf{77}\%$ accuracy for classifying Gleason scores. And our ordinal classifier achieves up to $\mathbf{82}\%$ for cancer T-Stage classification and $\mathbf{70}\%$ for Gleason score classification. The drop in accuracy for per-patient experiments compared with per-image ones is primary due to the decrease in data samples.

Among the 16% failure cases for cancer staging classification, 15% of our multinomial classification results with age feature is only 1 stage away from the ground truth. And for the failure cases for scoring classification, only 10% of the classified Gleason scores is 1 away from the ground truth and 13% of them are 2 away from the ground truth.

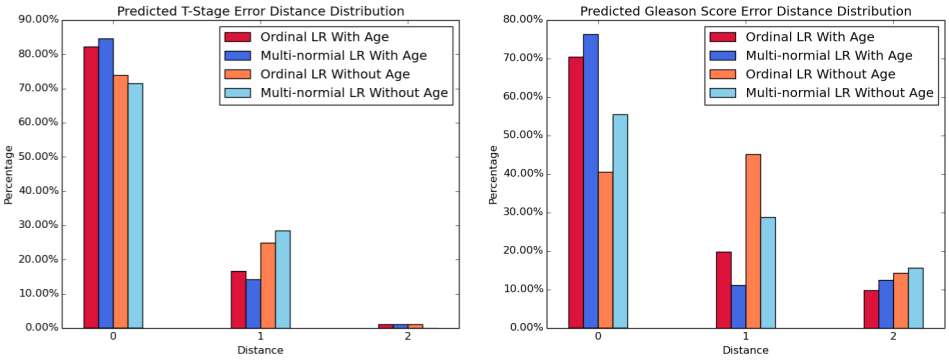

(a) (b)

Fig. 3. Error Distribution of Cancer Aggression/Staging Classification for Per-Patient Study. (a) shows the accuracy and error distribution of our recovered prostate elasticity parameter and cancer T-Stage. For our patient dataset, the multinomial classifier (shown in royal blue and sky blue) outperforms the ordinal classifier (shown in crimson and coral). We achieve up to $\mathbf{84}\%$ accuracy using multinomial logistic regression and $\mathbf{82}\%$ using ordinal logistic regression for classifying cancer T-Stage based on our recovered elasticity parameter and patient age information. (b) shows the correlation between the recovered relative elasticity parameter and the Gleason score. We achieve up to $\mathbf{77}\%$ accuracy using multinomial logistic regression and $\mathbf{70}\%$ using ordinal logistic regression for classifying Gleason score based on our recovered elasticity parameter and patient age information.

5.4 Bayesian-Based Material Parameter Estimation

For Bayesian-based parameter estimation, we estimate the posterior probability distribution of the parameters $\mathbf{w}_k$,

$$p(\mathbf{w}_k|\mathbf{y}_{1:n}) \tag{4}$$

based on the observations,

$$\mathbf{y}_{1:n} = \mathbf{y}_1, \mathbf{y}_2, \ldots, \mathbf{y}_n \tag{5}$$

To motivate our reason for choosing unscented Kalman Filter as the estimation method, we will first give a brief introduction of the Recursive Bayesian Estimation algorithm. Recursive Bayesian estimation algorithm filters the posterior probability density function recursively for new observations. According to Bayes' theorem, the posterior probability density can be expressed as,

$$p(\mathbf{w}_k|\mathbf{y}_{1:n}) = \frac{p(\mathbf{y}_n|\mathbf{w}_k)p(\mathbf{w}_k|\mathbf{y}_{1:n-1})}{p(\mathbf{y}_n|\mathbf{y}_{1:n-1})} \tag{6}$$

We will not give details on every term in Eqn. 6. We focus on the hidden parameter transition prior $p(\mathbf{w}_k|\mathbf{w}_{k-1})$ and the observation likelihood densities $p(\mathbf{y}_n|\mathbf{w}_k)$. The computation of the hidden parameter transition prior $p(\mathbf{w}_k|\mathbf{w}_{k-1})$ depends on the update function $\mathbf{f}(\mathbf{x};\mathbf{w})$. In our application, the state update function $\mathbf{f}(\mathbf{x};\mathbf{w})$ is nonlinear. Thus we need an approximation method.

The basic Kalman Filter models the densities in Eqn. 6 by Gaussian distributions. And it assumes that the state posterior probabilistic density can consistently be minimized by updating only the first (mean) and second order moments (covariance) of the true probabilistic densities. The extended Kalman Filter applies the basic Kalman Filter to nonlinear dynamic state-space system by first linearize it using Taylor series. This linearization affects the accuracy of the estimation process. The unscented Kalman Filter approaches the nonlinear problem differently. Instead of linearizing the system using Taylor series, it uses a general deterministic sampling framework, or the sigma-point approach. Thus we choose to use unscented Kalman Filter as our basic estimator for our dynamic elasticity-parameter estimation problem.

Unscented Kalman Filter for Parameter Estimation The unscented Kalman Filter [30] handles the nonlinear problem with the idea that it is easier to approximate a random variable than a non-linear function. Like both basic Kalman filter and extended Kalman filter, the unscented Kalman filter consists of two steps: the prediction step and the correction step. In order to do parameter estimation, we first construct a mapping between the measured observation $\mathbf{y}'$, state $\mathbf{x}$ and the parameters $\mathbf{w}$. In the following, we will use $\mathbf{d}$ for $\mathbf{y}'$. The observation $\mathbf{y}$ equals to the measured observation $\mathbf{d}$ when the state $\mathbf{x}$ and the parameters $\mathbf{w}$ are optimized. We define a function $\mathbf{g}$ as follows,

$$\mathbf{d}_k = \mathbf{g}(\mathbf{x}_k, \mathbf{w}_k) \tag{7}$$

We will use superscript minus for prior probabilistic densities, $\mathbf{P}$ for covariance matrix, hat symbol for the mean of the random variable, subscript k for the current estimation iteration and L as the size of the parameter vector $\mathbf{w}$.

1. Initialize the mean of the parameters and the covariance matrix of the parameters

$$\hat{\mathbf{w}}_0 = E[\mathbf{w}_0] \tag{8}$$

with $\mathbf{w}_0$ as the initial guess of the parameters

$$\mathbf{P}_{\mathbf{w}_0} = E[(\mathbf{w}_0 - \hat{\mathbf{w}}_0)(\mathbf{w}_0 - \hat{\mathbf{w}}_0)^T] \tag{9}$$

2. For each estimation iteration k: Compute the prior of the mean of the parameters and the prior of the covariance of the parameters as,

$$\hat{\mathbf{w}}_k^- = \hat{\mathbf{w}}_{k-1} \tag{10}$$

$$\mathbf{P}_{\mathbf{w}_k}^- = \mathbf{P}_{\mathbf{w}_{k-1}} \tag{11}$$

Select a set of sigma points $\mathcal{X}_{k|k-1}$. The columns of the matrix $\mathcal{X}_{k|k-1}$ are the sampled parameters.

$$\mathcal{X}_{k|k-1} = [\hat{\mathbf{w}}_k^-, \hat{\mathbf{w}}_k^- + \gamma\sqrt{\mathbf{P}_{\mathbf{w}_k}^-}, \hat{\mathbf{w}}_k^- - \gamma\sqrt{\mathbf{P}_{\mathbf{w}_k}^-}] \tag{12}$$

where $\gamma = \sqrt{L+\lambda}$. The matrix expands as,

$$\begin{aligned} \mathcal{X}_{0,k|k-1} &= \hat{\mathbf{w}}_k & i &= 0 \\ \mathcal{X}_{i,k|k-1} &= \hat{\mathbf{w}}_k + (\gamma\sqrt{\mathbf{P}_{\mathbf{w}_k^-}})_i & i &= 1,\ldots,L \\ \mathcal{X}_{i,k|k-1} &= \hat{\mathbf{w}}_k - (\gamma\sqrt{\mathbf{P}_{\mathbf{w}_k^-}})_i & i &= L+1,\ldots,2L \end{aligned} \tag{13}$$

The weights $\omega^{(m)}$ for computing the mean of the sigma-points and the weights $\omega^{(c)}$ for computing the covariance matrix of the sigma-points are,

$$\begin{aligned} \omega_0^{(m)} &= \tfrac{\lambda}{L+\lambda} & i &= 0 \\ \omega_0^{(c)} &= \tfrac{\lambda}{L+\lambda} + (1-\alpha^2+\beta) & i &= 0 \\ \omega_i^{(m)} &= \omega_i^{(c)} = \tfrac{1}{2(L+\lambda)} & i &= 1,\ldots,2L \end{aligned} \tag{14}$$

$$\sum_{i=0}^{i=2L} \omega_i^{(c)} = 1, \ \sum_{i=0}^{i=2L} \omega_i^{(m)} = 1 \tag{15}$$

where α and β are two tuned parameters for the filter. α affects the distribution of the sigma-points. The distribution of the sigma-points can affect the convergence rate to some extent. And β controls the tails of the posterior distribution. In our experiments we set $\beta = 2$ and α varies from 0.1 to 2. Then compute the measured observation sigma points of each element of the sigma points matrix $\mathcal{X}_{k|k-1}$,

$$\mathcal{Y}_{k|k-1} = \mathbf{g}(\mathbf{x}_k, \mathcal{X}_{k|k-1}) \tag{16}$$

the prior of the mean of the measurements $\mathbf{d}_k^-$,

$$\hat{\mathbf{d}}_k^- = \sum_{i=0}^{2L} \omega_i^{(m)} \mathcal{Y}_{i,k|k-1} \tag{17}$$

the prior of the covariance matrix of the measurements $\mathbf{P}_{\mathbf{d}_k}^-$,

$$\mathbf{P}_{\mathbf{d}_k}^- = \sum_{i=0}^{2L} \omega_i^{(c)} (\mathcal{Y}_{i,k|k-1} - \hat{\mathbf{d}}_k^-)(\mathcal{Y}_{i,k|k-1} - \hat{\mathbf{d}}_k^-)^T + \mathbf{R}_{\mathbf{e}_k} \tag{18}$$

the cross covariance matrix for the parameter and the measurement,

$$\mathbf{P}_{\mathbf{w}_k\mathbf{d}_k} = \sum_{i=0}^{2L} \omega_i^{(c)} (\mathcal{X}_{i,k|k-1} - \hat{\mathbf{w}}_k^-)(\mathcal{Y}_{i,k|k-1} - \hat{\mathbf{d}}_k^-)^T \tag{19}$$

Compute the Kalman gain $\mathbf{K}_k$,

$$\mathbf{K}_k = \mathbf{P}_{\mathbf{w}_k\mathbf{d}_k} \mathbf{P}_{\mathbf{d}_k}^{-1} \tag{20}$$

Compute the posterior of the parameter and the posterior covariance of the parameter

$$\mathbf{w}_k = \mathbf{w}_k^- + \mathbf{K}_k(\mathbf{y}_n - \hat{\mathbf{d}}_k^-) \tag{21}$$

$$\mathbf{P}_{\mathbf{w}_k} = \mathbf{P}_{\mathbf{w}_k}^- - \mathbf{K}_k \mathbf{P}_{\mathbf{d}_k} \mathbf{K}_k^T \tag{22}$$

Coupled State Estimation The hidden state variables for our dynamical system include the positions, the velocities, and the accelerations. Though the unscented Kalman Filter can be used for dual state-parameter estimation, the fact that the state and the parameters are coupled makes such a dual estimation fail to converge. Thus we use the finite difference method to estimate both the initial velocities and the accelerations. Given the observations of three frames $\mathbf{y}_{n-1}$, $\mathbf{y}_n$, $\mathbf{y}_{n+1}$ and the time elapsed between the frames Δt, the velocities $\dot{\mathbf{u}}$,

$$\dot{\mathbf{u}} = \frac{\mathbf{y}_n - \mathbf{y}_{n-1}}{\Delta t} \tag{23}$$

the accelerations $\ddot{\mathbf{u}}$,

$$\ddot{\mathbf{u}} = \frac{\mathbf{y}_{n+1} - 2\mathbf{y}_n + \mathbf{y}_{n-1}}{(\Delta t)^2} \tag{24}$$

Our dynamic parameter estimation scheme is given in Algorithm 1.

Algorithm 1 Dynamic Elasticity Parameter Estimation

procedure MEASUREMENT COMPUTATION
  // this is the function $\mathbf{g}$ in Eqn. 8.
  $\dot{\mathbf{u}} \leftarrow (\mathbf{y}_n - \mathbf{y}_{n-1})/\Delta t$
  $\ddot{\mathbf{u}} \leftarrow (\mathbf{y}_{n+1} - 2\mathbf{y}_n + \mathbf{y}_{n-1})/(\Delta t)^2$
  $\mathbf{d} \leftarrow \mathbf{f}(\mathbf{x}; \mathbf{w})$ // evaluate measurement based on the parameters and the states
end Measurement Computation;
procedure UNSCENTED KALMAN FILTER ITERATE
  $\mathcal{X}_{k|k-1} \leftarrow [\hat{\mathbf{w}}_k^-, \hat{\mathbf{w}}_k^- + \gamma\sqrt{\mathbf{P}_{\mathbf{w}_k}^-}, \hat{\mathbf{w}}_k^- - \gamma\sqrt{\mathbf{P}_{\mathbf{w}_k}^-}]$
  // compute the sigma-points
  $\mathcal{Y}_{k|k-1} \leftarrow \mathbf{g}(\mathbf{x}_n, \mathbf{w}_k^-)$ // compute the prior of the mean of the measurement sigma-points
  $\hat{\mathbf{d}}_k^- \leftarrow \sum_{i=0}^{2L} \omega_i^{(m)} \mathcal{Y}_{i,k|k-1}$ // compute the prior of the covariance matrix of the measurement sigma-points
  $\mathbf{P}_{\mathbf{w}_k\mathbf{d}_k} \leftarrow \sum_{i=0}^{2L} \omega_i^{(c)} (\mathcal{X}_{i,k|k-1} - \hat{\mathbf{w}}_k^-)(\mathcal{Y}_{i,k|k-1} - \hat{\mathbf{d}}_k^-)^T$ // compute the cross covariance matrix of the measurements and the parameters
  $\mathbf{K}_k \leftarrow \mathbf{P}_{\mathbf{w}_k\mathbf{d}_k} \mathbf{P}_{\mathbf{d}_k}^{-1}$ // compute the Kalman gain
  $\hat{\mathbf{w}}_k \leftarrow \mathbf{w}_k^- + \mathbf{K}_k(\mathbf{y}_n - \hat{\mathbf{d}}_k^-)$
  // update the mean of the parameters
  $\mathbf{P}_{\mathbf{w}_k} \leftarrow \mathbf{P}_{\mathbf{w}_k}^- - \mathbf{K}_k \mathbf{P}_{\mathbf{d}_k} \mathbf{K}_k^T$
  // update the covariance matrix of the parameters
end Unscented Kalman Filter Iterate;
procedure MAIN
  while not converged **do**
    for Sampled Keyframes $\mathbf{y}_{n_i}$ **do**
      Initialize $\mathbf{x}_0$, $\mathbf{w}_0$, $\mathbf{P}_{\mathbf{w}_0}$
      Unscented Kalman Filter Iterate()
    end for;
  end while;
end Main;

6 Progress to Date and Remaining Tasks

Much of the work has already been completed.

- Image-based multi-region mechanical property recovery [36,35]
- Video-based dynamic non-rigid body mechanical property recover [37]
- Mechanical property recovery for cancer stage correlation study [34]
- Video-based garment mechanical property recovery [33]

References

1. Ashab, H.A.D., Haq, N.F., Nir, G., Kozlowski, P., Black, P., Jones, E.C., Goldenberg, S.L., Salcudean, S.E., Moradi, M.: Multimodal classification of prostate tissue: a feasibility study on combining multiparametric mri and ultrasound. In: SPIE Medical Imaging. pp. 94141B–94141B. International Society for Optics and Photonics (2015)
2. Balocco, S., Camara, O., Frangi, A.F.: Towards regional elastography of intracranial aneurysms. In: Medical Image Computing and Computer-Assisted Intervention. vol. 11, pp. 131–8 (2008), http://www.ncbi.nlm.nih.gov/pubmed/18982598, PMID: 18982598
3. Becker, M., Teschner, M.: Robust and efficient estimation of elasticity parameters using the linear finite element method. Proc. of Simulation and Visualization pp. 15–28 (2007)
4. Bhat, K.S., Twigg, C.D., Hodgins, J.K., Khosla, P.K., Popovic, Z., Seitz, S.M.: Estimating cloth simulation parameters from video. In: Proceedings of the 2003 ACM SIGGRAPH/Eurographics symposium on Computer animation. pp. 37–51. Eurographics Association Aire-la-Ville, Switzerland (2003)
5. Bickel, B., Bächer, M., Otaduy, M.A., Matusik, W., Pfister, H., Gross, M.: Capture and modeling of non-linear heterogeneous soft tissue. In: ACM SIGGRAPH 2009 papers. pp. 1–9. ACM, New Orleans, Louisiana (2009), http://portal.acm.org/citation.cfm?id=1531395
6. Cotin, S., Delingette, H., Ayache, N.: Real-time elastic deformations of soft tissues for surgery simulation. Visualization and Computer Graphics, IEEE Transactions on 5(1), 62–73 (1999)
7. Dubuisson, M.P., Jain, A.K.: A modified hausdorff distance for object matching. In: Pattern Recognition, 1994. Vol. 1-Conference A: Computer Vision & Image Processing., Proceedings of the 12th IAPR International Conference on. vol. 1, pp. 566–568. IEEE (1994)
8. Engl, H.W., Kunisch, K., Neubauer, A.: Convergence rates for tikhonov regularisation of non-linear ill-posed problems. Inverse problems 5(4), 523 (1989)
9. Fu, D., Levinson, S., Gracewski, S., Parker, K.: Non-invasive quantitative reconstruction of tissue elasticity using an iterative forward approach. PHYSICS IN MEDICINE AND BIOLOGY 45(6), 1495–1510 (2000)
10. Golub, G.H., Hansen, P.C., O'Leary, D.P.: Tikhonov regularization and total least squares. SIAM Journal on Matrix Analysis and Applications 21(1), 185–194 (1999)
11. Kallel, F., Bertrand, M.: Tissue elasticity reconstruction using linear perturbation method. Medical Imaging, IEEE Transactions on 15(3), 299–313 (1996)
12. Khojaste, A., Imani, F., Moradi, M., Berman, D., Siemens, D.R., Sauerberi, E.E., Boag, A.H., Abolmaesumi, P., Mousavi, P.: Characterization of aggressive prostate cancer using ultrasound rf time series. In: SPIE Medical Imaging. pp. 94141A–94141A. International Society for Optics and Photonics (2015)

13. Liu, Y., Storey, C.: Efficient generalized conjugate gradient algorithms, part 1: theory. Journal of Optimization Theory and Applications 69(1), 129–137 (1991)
14. Miguel, E., Bradley, D., Thomaszewski, B., Bickel, B., Matusik, W., Otaduy, M., Marschner, S.: Data-driven estimation of cloth simulation models. Computer Graphics Forum (Eurographics 2012) 31(2) (2012)
15. Miguel, E., Tamstorf, R., Bradley, E., Schvartzman, S., Thomaszewski, B., Bickel, B., Matusik, W., Marschner, S., Otaduy, M.: Modeling and estimation of internal friction in cloth. ACM Transactions on Graphics (Proc. SIGGRAPH Asia) 32(6) (2013)
16. Müller, M., Gross, M.: Interactive virtual materials. In: Proceedings of Graphics Interface 2004. p. 239–246. GI '04, Canadian Human-Computer Communications Society, School of Computer Science, University of Waterloo, Waterloo, Ontario, Canada (2004), http://dl.acm.org/citation.cfm?id=1006058.1006087
17. Muthupillai, R., Ehman, R.L.: Magnetic resonance elastography. Nat Med 2(5), 601–603 (May 1996), http://dx.doi.org/10.1038/nm0596-601
18. Nealen, A., Muller, M., Keiser, R., Boxerman, E., Carlson, M.: Physically based deformable models in computer graphics. Computer Graphics Forum 25, 809–836 (2006)
19. Ophir, J., Alam, S., Garra, B., Kallel, F., Konofagou, E., Krouskop, T., Varghese, T.: Elastography: ultrasonic estimation and imaging of the elastic properties of tissues. Proceedings of the Institution of Mechanical Engineers, Part H: Journal of Engineering in Medicine 213(3), 203–233 (Jan 1999), http://dx.doi.org/10.1243/0954411991534933
20. Pai, D.K., Doel, K.v.d., James, D.L., Lang, J., Lloyd, J.E., Richmond, J.L., Yau, S.H.: Scanning physical interaction behavior of 3D objects. In: Proceedings of SIGGRAPH 2001. p. 87–96. SIGGRAPH '01, ACM, New York, NY, USA (2001), http://doi.acm.org/10.1145/383259.383268
21. Press, W.H.: Numerical recipes. Cambridge University Press (2007)
22. Rivaz, H., Boctor, E., Foroughi, P., Zellars, R., Fichtinger, G., Hager, G.: Ultrasound elastography: A dynamic programming approach. Medical Imaging, IEEE Transactions on 27(10), 1373–1377 (2008)
23. Rivlin, R.S., Saunders, D.: Large elastic deformations of isotropic materials. vii. experiments on the deformation of rubber. Philosophical Transactions of the Royal Society of London. Series A, Mathematical and Physical Sciences 243(865), 251–288 (1951)
24. Saad, Y., Schultz, M.H.: Gmres: A generalized minimal residual algorithm for solving nonsymmetric linear systems. SIAM Journal on scientific and statistical computing 7(3), 856–869 (1986)
25. Schnur, D.S., Zabaras, N.: An inverse method for determining elastic material properties and a material interface. International Journal for Numerical Methods in Engineering 33(10), 2039–2057 (1992), http://dx.doi.org.libproxy.lib.unc.edu/10.1002/nme.1620331004
26. Skovoroda, A., Emelianov, S.: Tissue elasticity reconstruction based on ultrasonic displacement and strain images. IEEE Transactions on Ultrasonics, Ferroelectrics, and Frequency Control 42(4), 141 (1995)
27. Syllebranque, C., Boivin, S.: Estimation of mechanical parameters of deformable solids from videos. The Visual Computer 24(11), 963–972 (2008)
28. Teschner, M., Heidelberger, B., Manocha, D., Govindaraju, N., Zachmann, G., Kimmerle, S., Mezger, J., Fuhrmann, A.: Collision handling in dynamic simulation environments: The evolution of graphics: Where to next? In: Eurographics 2005 Tutorial (2005)
29. Treloar, L.R., Hopkins, H., Rivlin, R., Ball, J.: The mechanics of rubber elasticity [and discussions]. Proceedings of the Royal Society of London. A. Mathematical and Physical Sciences 351(1666), 301–330 (1976)

30. Wan, E., Van Der Merwe, R., et al.: The unscented kalman filter for nonlinear estimation. In: Adaptive Systems for Signal Processing, Communications, and Control Symposium 2000. AS-SPCC. The IEEE 2000. pp. 153–158. IEEE (2000)
31. Wang, H., Ramamoorthi, R., O'Brien, J.: Data-driven elastic models for cloth: Modeling and measurement. ACM Transactions on Graphics (SIGGRAPH) 30(4), 71:1–71:12 (2011)
32. Washington, C.W., Miga, M.I.: Modality independent elastography (MIE): a new approach to elasticity imaging. IEEE Trans. on Medical Image 23(9), 1117–1128 (2004)
33. Yang, S., Ambert, T., Pan, Z., Wang, K., Yu, L., Berg, T., Lin, M.C.: Detailed garment recovery from a single-view image. arXiv preprint arXiv:1608.01250 (2016)
34. Yang, S., Jojic, V., Lian, J., Chen, R., Zhu, H., Lin, M.C.: Classification of prostate cancer grades and t-stages based on tissue elasticity using medical image analysis. In: International Conference on Medical Image Computing and Computer-Assisted Intervention. pp. 627–635. Springer (2016)
35. Yang, S., Lin, M.: Materialcloning: Acquiring elasticity parameters from images for medical applications (2015)
36. Yang, S., Lin, M.: Simultaneous estimation of elasticity for multiple deformable bodies. Computer animation and virtual worlds 26(3-4), 197–206 (2015)
37. Yang, S., Lin, M.C.: Bayesian estimation of non-rigid mechanical parameters using temporal sequences of deformation samples. In: Robotics and Automation (ICRA), 2016 IEEE International Conference on. pp. 4036–4043. IEEE (2016)
38. Zhu, Y., Hall, T., Jiang, J.: A finite-element approach for young's modulus reconstruction. Medical Imaging, IEEE Transactions on 22(7), 890–901 (2003)
39. Zienkiewicz, O.C., Taylor, R.L.: The Finite Element Method. Butterworth-Heinemann, Oxford, 6 edn. (Dec 2005)